

REPORT DOCUMENTATION PAGE

AFRL-SR-AR-TR-06-0469

The public reporting burden for this collection of information is estimated to average 1 hour per response, including the time for gathering and maintaining the data needed, and completing and reviewing the collection of information. Send comments regarding this burden estimate or any other aspect of this collection of information, including suggestions for reducing the burden, to the Department of Defense, Executive Service and Community Affairs, Washington, DC 20301-4070. Send all other correspondence regarding this collection of information to the Office of Management and Budget, Paperwork Project Director (0142-0046), Washington, DC 20503-9042.

PLEASE DO NOT RETURN YOUR FORM TO THE ABOVE ORGANIZATION.

1. REPORT DATE (DD-MM-YYYY) 02/28/2006		2. REPORT TYPE Final Report		3. DATES COVERED (From - To) 08/01/2003 - 02/28/2006	
4. TITLE AND SUBTITLE "Direct Printing of Organic Electronics at the Nanometer Scale"				5a. CONTRACT NUMBER F49620-03-1-0410	
				5b. GRANT NUMBER	
				5c. PROGRAM ELEMENT NUMBER	
6. AUTHOR(S) Stephen R. Forrest				5d. PROJECT NUMBER	
				5e. TASK NUMBER	
				5f. WORK UNIT NUMBER	
7. PERFORMING ORGANIZATION NAME(S) AND ADDRESS(ES) Princeton University, Princeton, NJ				8. PERFORMING ORGANIZATION REPORT NUMBER	
9. SPONSORING/MONITORING AGENCY NAME(S) AND ADDRESS(ES) Air Force Office of Scientific Research 4015 Wilson Blvd Room 713 Arlington, VA 22203-1954					
<div style="font-size: 2em; font-weight: bold;">20061130013</div>					
12. DISTRIBUTION/AVAILABILITY STATEMENT <i>Distribution Statement A: unlimited</i>					
13. SUPPLEMENTARY NOTES					
14. ABSTRACT We explore new methods for direct patterned growth of organic semiconductor thin films useful in organic electronic devices. The scope of the program ranged from the growth of patterns from the nanometer to the centimeter scales. Its objectives included developing new tools and analytical techniques for the fabrication of organic nano- and microstructures, to the study of such low dimensionality nanostructures for their interesting and potentially useful optoelectronic properties. The work included fundamental theoretical and experimental investigations of the limitations to growth at the smallest dimensions (~10nm), and applying these findings to the demonstration of practical organic electronic devices. We demonstrate direct patterning of very high performance electrophosphorescent organic light emitting devices and scaling up of the printing apparatus for direct patterning of multiple devices simultaneously.					
15. SUBJECT TERMS					
16. SECURITY CLASSIFICATION OF:			17. LIMITATION OF ABSTRACT	18. NUMBER OF PAGES 15	19a. NAME OF RESPONSIBLE PERSON Stephen Forrest
a. REPORT	b. ABSTRACT	c. THIS PAGE			19b. TELEPHONE NUMBER (Include area code) 734-647-1147

Best Available Copy

## Objectives

Low pressure organic vapor phase deposition (OVPD) developed at Princeton University under past support from AFOSR affords a completely new method for the precise deposition of molecular organic thin film nanostructures with many features unavailable to other deposition techniques such as vacuum thermal evaporation (VTE) and ultrahigh vacuum organic molecular beam deposition (OMBD) – the latter process also pioneered by our laboratory. Sharing several characteristics and advantages of vapor phase epitaxy used successfully in the growth of III-V and II-VI semiconductors, OVPD allows for precise control of the organic layer structure over very large substrate areas (exceeding 30 cm diameter), allows for the deposition of pure amorphous and polycrystalline films in a controlled environment, and most significantly, allows for highly precise, simultaneous doping of numerous molecular species into an organic host film. More directly relevant to the present proposed program, we have recently shown that OVPD is capable of growth of very small patterns of organic thin films, with resolutions to  $<1\mu\text{m}$ [2]. This has led to the suggestion that a modified form of OVPD, called organic vapor jet printing (OVJP), may be useful for the growth of structures down to the nanometer scale. Preliminary experiments at Princeton University have demonstrated the feasibility of this highly versatile and novel direct printing process.

Based on these findings, the objective of this program is to push the limits of patterned growth of organic thin films to generate wires and other structures consisting of possibly only a single file of organic molecules, deposited only one or a few layers deep. The process may ultimately be adapted to the growth of inorganic semiconductors such as Ge

and Si, resulting in direct printing of both organic and inorganic quantum structures whose placement can be precisely controlled. We, therefore, will have an unprecedented opportunity to study phenomena and technology at the single and few-molecule scales. Our objectives are two-fold: to develop ultrahigh resolution tools for the growth of molecular organic thin films, and to study the properties of these deposits which are clearly in the "quantum domain".

In addition to being an excellent tool for research on organic films, OVPD has caught the interest of the industrial sector. In particular, **Aixtron, AG** (Aachen, Germany), the largest world-wide manufacturer of metallorganic chemical vapor deposition systems, has teamed with **Universal Display Corporation** (Ewing, NJ) to produce OVPD equipment to be used in the large-scale manufacture of emissive displays employing molecular organic light emitting devices (OLEDs). These machines, the first of which is currently being successfully operated at UDC, should be made generally available in 2003 to the manufacturing sector. Prof. Forrest has been deeply involved in the design and construction of this equipment, and has played a role in the transition of OVPD from its first conception to its full commercialization. During the course of this program, our team will work closely with our industrial partners, **Aixtron AG** and **Universal Display Corp.**, to develop an OVPD research apparatus that will be useful to a range of researchers interested in display and other organic thin film electronics devices.

## Publications

1. "The Path to Ubiquitous and Low Cost Organic Electronic Appliances on Plastic", S. R. Forrest, *Nature* (London), invited, **428**, 911 (2004).
2. "Direct printing of molecular organic semiconductors for molecular electronics", M. Shtein, P. Peumans, J. B. Benziger and S. R. Forrest, *Adv. Mat.*, **16**, 1615 (2004).
3. "Direct mask-free patterning of molecular organic semiconductors using organic vapor jet printing", M. Shtein, P. Peumans, J. B. Benziger and S. R. Forrest, *J. Appl. Phys.*, **96**, 4500 (2004).
4. "Controlled growth of a molecular bulk heterojunction photovoltaic cell", F. Yang, M. Shtein, and S. R. Forrest, *Nat. Mater.*, **4**, 39 (2004).
5. "Stable and efficient electrophosphorescent organic light emitting devices grown by organic vapor phase deposition", T. X. Zhou, T. Ngo, J. J. Brown, M. Shtein and S. R. Forrest, *Appl. Phys. Lett.*, **86**, 021107 (2005).
6. "Direct Patterning of Organic Light Emitting Devices by Organic Vapor Jet Printing", Y. Sun, M. Shtein, and S. R. Forrest, *Appl. Phys. Lett.*, **86** 113504 (2005).
7. "Morphology control and material mixing by high-temperature organic vapor phase deposition and its application to thin-film solar cells", F. Yang, M. Shtein and S. R. Forrest, *J. Appl. Phys.*, **98**, 014906 (2005).

## Presentations

1. "Organic vapor jet printing for direct patterning of small-molecule organic-based electronics", M. Shtein, P. Peumans, J. Benziger and S. R. Forrest, MRS Ann. Mtg., Paper M12.7, Boston (Dec., 2003).
2. "Growth of Thin Films by Organic Vapor Phase Deposition and Related Techniques", M. Shtein, P. Peumans, J. Benziger and S. R. Forrest, Soc. Inf. Display-MAC, NJ (Oct., 2003)
3. "Organic Optoelectronics: Is it for real or is it just another fad?", S. R. Forrest, invited, AAAS Annual Meeting, Seattle (Feb., 2004).
4. "Process controllability and stability in organic vapor phase deposition", M. Schwambersa, M. Gersdorff, M. Reinhold, N. Meyer, G. Strauch, B. Marheineke, M. Heuken, T. X. Zhou, T. Ngo, J. J. Brown, M. Shtein and S. R. Forrest, Asia Display/IMID '04, Paper 18.6, Daegu, Korea (Aug. 23-27, 2004).

5. "High Efficiency Bulk Heterojunction Photovoltaic Cells Grown by Organic Vapor Phase Deposition", F. Yang, M. Shtein and S. R. Forrest, MRS Fall Mtg., Paper L4.4, Boston (Nov., 2004).
6. "Organic Vapor Phase and Organic Vapor Jet Deposition of OLEDs and Photovoltaic Cells", S. R. Forrest, F. Yang, Y. Sun and M. Shtien, invited, SIDMAC 04, NJ (Nov. 3, 2004).
7. "Organic Electronics: New Materials, Physics and Devices for Modern Optoelectronics", S. R. Forrest, Deutsche Physicalische Gesellschaft (German Physical Society), plenary, Berlin (March, 2005).

### **Personnel supported and/or associated with the research project**

Post Doctoral Researcher: Yohai Roichman

Graduate Students: Brian D'Andrade  
Jiangeng Xue  
Russell Holmes  
Mahima Gupta  
Xin Xu  
Mengmeng Yu

### **Invention Disclosures for the AFOSR Program**

1. Homogeneously Mixed Bulk Heterojunction
2. Improved Power Conversion Efficiency of Organic Donor-Acceptor Photovoltaic Cells
3. Organic Light Emitting Diodes (OLED) Grown on SN02 Coated Glass
4. Photovoltaic Fiber
5. Solvent-Free Jet Printing

## **Transitions**

All results in this program have been successfully transferred to **Universal Display Corp.** who is the sole, world wide licensee of the intellectual property developed by the PI at **Princeton University**. UDC has had a continuous presence in the PI's laboratory at Princeton since 1994, with company engineers working alongside students to ensure a continuous and seamless transfer of technology as it is developed. Furthermore, UDC has strong and close contacts with several DoD research laboratories, most particularly **AFRL**. Hence, technologies developed in this program have a rapid route to transfer directly to the DoD user. The PI himself has frequent and direct contact with AFRL personnel through this UDC-based relationship.

In addition, **Aixtron, AG**, a licensee of UDC, has manufactured and qualified organic vapor phase deposition tools for use in the display manufacturing industry. These tools, capable of large scale and rapid production of organic light emitting displays, have been engineered with close collaboration and assistance of the PI and his students during the course of this program.

Overall, the transition of technology during the course of this program has been highly successful and complete. The transitions are continuing to be completed even beyond the term of this project.

## Summary of Results

The use of organic semiconductors in devices is a bustling technology especially in the area of organic light emitting devices (OLEDs). Due to the relatively weak Van der Waals bonding of the molecules, organic semiconductors can be deposited on various substrates without the need for lattice matching. In addition, organic molecules can be engineered through a wide range of energy levels allow us to tune the absorption, emission, and transport properties of devices easily. Patterning of organic semiconductors has also become increasingly important. Because we are unable to do photolithography on organics, without direct patterning the only other option is vacuum thermal evaporation (VTE) with shadow masking. Fabricating devices such as thin film transistors (TFTs) and full color OLED displays would require multiple costly alignment and masking steps as seen in Figure 1.

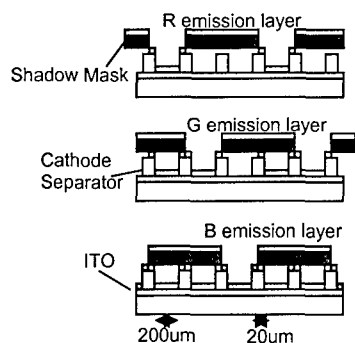


Figure 1: Fabrication steps for a full color OLED display

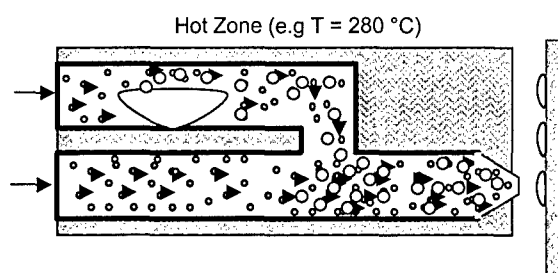


Figure 2: Basic OVJP concept

To avoid these lengthy processes the technology of Organic Vapor Jet Printing (OVJP) was developed. As depicted in Figure 2, in OVJP organic material is brought to its sublimation point. Then a hot inert carrier gas flows past the material and through a

series of collisions, it carries the organic vapor down stream to a nozzle. The organic vapor and carrier gas mixture then exits the nozzle which is in close proximity to a cool substrate. The organic molecules condense on the substrate in a well defined deposit while the inert carrier gas flows past the substrate. Using the 1<sup>st</sup> generation OVJP, it was shown to be able to achieve precise patterning as seen in Figure 3. Also, a flat film OVJP grown Alq<sub>3</sub>/NPD OLED was shown to be competitive with VTE with quantum efficiencies of 0.84%.

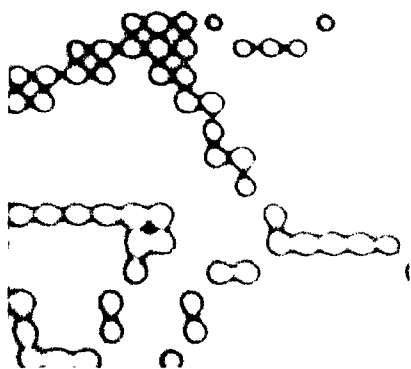


Figure 3: Patterning with 1<sup>st</sup> Generation OVJP with 10um diameter nozzle.

To further explore the device fabrication applications of OVJP, we demonstrated that it could be used to print uniform, (1cm)<sup>2</sup> flat organic thin films, as well as to deposit patterned, organic heterostructure devices. By using a nozzle array, OVJP is used to simultaneously print multiple stripes of organic semiconductors, broadening the range of patterning functions and illustrating that the various organic components can be rapidly deposited in parallel. In particular, we fabricate high-performance fluorescent OLEDs consisting of the broad area printing of a 4,4'-bis[N-(1-naphthyl)-N-phenyl-amino]-biphenyl ( $\alpha$ -NPD) hole transport layer, followed by stripes of a tris(8-hydroxyquinoline)-aluminum (Alq<sub>3</sub>) electron transport and emitting layer. The OLEDs exhibited an external

quantum efficiency of  $(0.84 \pm 0.03)\%$ , consistent with values obtained by conventional vacuum thermal evaporation.

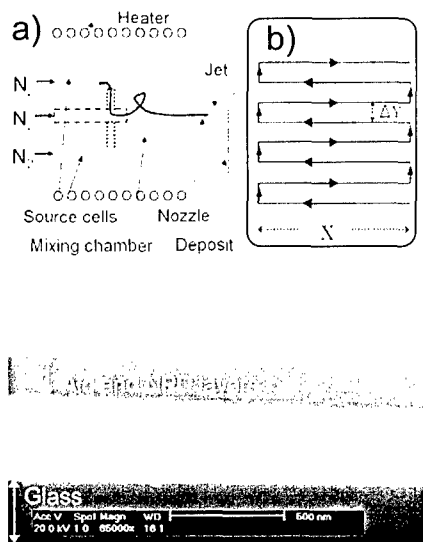


Fig. 4. (a) Schematic of the organic vapor jet printing (OVJP) apparatus, shown with two of the five source cells used, a center dilution channel, and a modular collimating nozzle, all heated from the outside. A hot inert carrier gas enters the apparatus, picks up the organic vapor, and ejects the gas mixture through the nozzle. The collimated vapor jet impinges onto a cooled substrate where the organic molecules selectively physisorb. (b) Schematic of the translation path of the substrate in an X-Y plane perpendicular to the jet direction. Translation in X is at a constant speed, and the switching time from line to line in Y is  $< 0.6$  s.  $\Delta Y$  denotes the spacing of lines which is adjustable. (c) Scanning electron micrograph of a cross section of an organic heterostructure printed on an ITO glass substrate using a  $340 \mu\text{m}$  diameter nozzle, showing a nearly featureless flat surface.

The OVJP apparatus (Fig. 4a) consists of a uniformly heated stainless steel cylindrical print head housing five separate source cells, a central dilution channel, a mixing chamber, and one or more outlet nozzles. Each cell can contain a separate molecular species, while the cell outlets connect via the mixing chamber. The head is mounted in a stainless steel chamber maintained at 0.11 Torr by means of a roughing pump, with a total nitrogen carrier gas flow rate of 4 sccm. Three types of nozzles were used: One with a nominal inside diameter of  $340 \mu\text{m}$  and a flow channel length of  $2000 \mu\text{m}$  (Type I); an array of three  $640 \mu\text{m}$  diameter by  $800 \mu\text{m}$  long nozzles with a center-to-center spacing of  $1410 \mu\text{m}$  (Type II-a), and  $2100 \mu\text{m}$  (Type II-b); and an array of three  $600 \mu\text{m} \times 6000 \mu\text{m}$  slits with  $800 \mu\text{m}$  thick wall and with a center-to-center spacing of  $1410 \mu\text{m}$  (Type III). The substrates were mounted onto a water-cooled holder attached to

a computer-controlled XYZ-positioning stage. The nozzle and the heated source cells remain stationary, while the substrate is translated continuously at a constant speed perpendicular to the jet direction in a path illustrated in Fig. 4(b). Sweeping the nozzle in this pattern is used to deposit a flat thin film.

Devices were grown on glass substrates pre-coated with a 150-nm-thick layer of indium tin oxide (ITO) with a sheet resistance of 20  $\Omega$ /sq. Substrates were ultrasonically cleaned in detergent solution for approximately 1 min., followed by thorough rinse in deionized water. They were then boiled in 1,1,1-trichloroethane, followed by drying in pure nitrogen, and then rinsed sequentially in acetone and isopropanol, and then once again dried in pure nitrogen gas. Substrates were exposed to an ultraviolet-ozone ambient for 5 minutes immediately prior to film deposition. Both the  $\alpha$ -NPD and Alq<sub>3</sub> layers were printed in succession in OVJP without exposure to air. The sample was then placed in a vacuum chamber where an array of 0.3 mm diameter cathodes consisting of a 0.8 nm thick layer of LiF followed by a 60 nm thick layer of Al were deposited through a shadow mask. The OLEDs were tested in ambient, in the dark, using a Hewlett-Packard 4156C semiconductor parameter analyzer and a Newport Model 2932-C dual-channel power meter.

An OLED having the layer structure: ITO/60nm NPD/60nm Alq<sub>3</sub>/LiF:Al was deposited using a Type I nozzle, source temperatures of 247°C and 240°C for NPD and Alq<sub>3</sub>, respectively, and a substrate temperature of 15°C. The nozzle-to-substrate distance was  $s = 380 \mu\text{m}$  for depositing broad area flat films, and  $s = 60 \mu\text{m}$  for depositing stripes. The substrate translation speed was 557  $\mu\text{m/s}$ . Printing 30 10-mm-long lines with a center-to-center spacing of 320  $\mu\text{m}$  resulted in a (1cm)<sup>2</sup> thin film with a flat surface. Due

to overlap of adjacent passes of the nozzle, no swath boundaries due to sweeping were observed by optical microscopy. These conditions correspond to a growth rate of  $1.1 \text{ \AA}\cdot\text{cm}^2/\text{s}$ . Using a Type II-a nozzle array resulted in a tripling of the growth rate, as expected. A scanning electron microscope (SEM) image (Fig. 4(c)) of the organic heterostructure cross-section exhibits a flat thin film deposit with a root-mean-square (RMS) roughness of  $1.23\text{nm}$ , as determined using an atomic force microscope scanned across a  $(20 \mu\text{m})^2$  area.

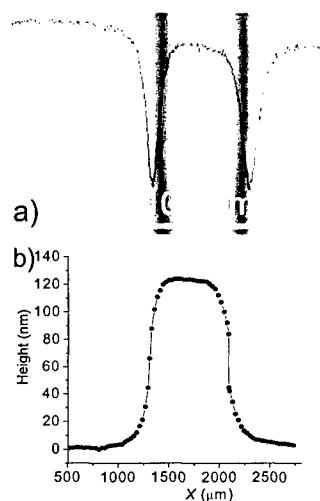


Fig. 5. (a) Optical micrograph of one of the parallel Alq<sub>3</sub> stripes simultaneously printed on a Si substrate using a Type II-b nozzle array. The curve is a scan of the optical interference fringe intensity obtained for the stripe under 440 nm wavelength illumination. (b) Thickness profile of the stripe deposit in (a) calculated according to the optical interference intensity.

Figure 5(a) is an optical microscope image of one of three parallel stripes grown using a Type II-b nozzle in a single pass, with other conditions similar to those used for the film in Fig. 4. Figure 5(b) shows the deposit thickness profile calculated from the optical interference intensity obtained under monochromatic light illumination at a wavelength of 440 nm. The three parallel organic heterostructure stripes have thicknesses of  $(123 \pm 8) \text{ nm}$ , and full-widths at half-maxima of  $(780 \pm 40) \mu\text{m}$ , compared with a nominal nozzle diameter of  $a = 640 \mu\text{m}$ . The approximate width of the usable, flat surface region of the stripe is approximately  $680 \mu\text{m}$ . The spread of approximately  $50 \mu\text{m}$  on

each side of the stripe is consistent with modeling of organic vapor phase deposition of organic films through square-edged shadow mask apertures using similar values of  $s$ ,  $P$  and  $a$ , employed in these experiments. This suggests that printing using nozzles where  $a > s$  is diffusion, rather than kinetically limited – the latter case applying to earlier work on OVJP with small diameter nozzles.

To fabricate OLEDs, we deposited an organic heterostructure consisting of a 50 nm thick, flat  $\alpha$ -NPD thin film printed by scanning a Type III nozzle across the substrate. This was followed by printing a 60 nm thick Alq<sub>3</sub> stripe layer using the same nozzle in a single sweep. The device was completed by cathode deposition in vacuum. Two similar control devices were deposited by vacuum thermal evaporation: one device was never exposed to air during deposition, and the second was exposed to air for 8 minutes between the Alq<sub>3</sub> layer and the LiF/Al cathode deposition steps. This approximately replicates the procedure used while transporting the OVJP grown films into the vacuum chamber for cathode deposition.

The performance characteristics of OLEDs on the three simultaneously OVJP-printed parallel stripes are compared with those of the air-exposed vacuum deposited device in Fig. 6. The OLEDs located in the striped regions exhibit quantum efficiency characteristics consistent to within experimental error with their vacuum-deposited but air-exposed analogs, with a maximum external quantum efficiency of  $(0.84 \pm 0.03)\%$ . At  $10\text{mA/cm}^2$ , the voltage of the OVJP device is  $V = (9.2 \pm 0.1)\text{V}$ , is  $(2.6 \pm 0.9)\text{V}$  higher than that for the unexposed vacuum deposited OLED. This difference is likely due to the organic layers of OVJP devices being thicker than those of the control devices. The

electroluminescent spectrum of the OVJP device peaks at  $\lambda = 519$  nm, with a half-width of  $\Delta\lambda = 55$  nm, consistent with expectations for Alq<sub>3</sub> emission.

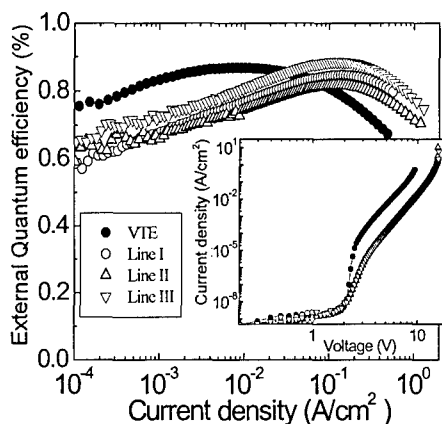


Fig. 6. External quantum efficiency versus current density characteristics of OLEDs on each of three simultaneously printed Alq<sub>3</sub> stripes printed on a broad area printed NPD film on ITO, compared with similar devices deposited in vacuum with the surface of Alq<sub>3</sub> layer exposed to air for 8 min. prior to deposition of metal contacts. Inset: Current density versus voltage characteristics for the same devices.

Analysis of the performance of the two types of vacuum deposited OLEDs indicates that exposure to air between deposition of Alq<sub>3</sub> and LiF results in a significant decrease in external quantum efficiency. For example, the unexposed sample has a maximum quantum efficiency of  $(1.16 \pm 0.02)\%$ , while the maximum quantum efficiency of the air-exposed OLED dropped by 30%, to  $(0.85 \pm 0.04)\%$  -- a value comparable to that obtained via printing.

Given the difference between the results of the unexposed and air-exposed OLEDs deposited in vacuum, we can expect that the quantum efficiency of the OLEDs printed by OVJP can be further improved by preventing exposure of the printed organic layers to air prior to metal cathode deposition. This can be achieved if the samples are transferred between the OVJP and the vacuum chambers through a nitrogen filled glove box.

Note that the patterning resolution reported here is lower than the typical requirements for practical OLED displays with  $100 \mu\text{m}$  diameter subpixels separated by at least  $10\text{-}20 \mu\text{m}$  wide gaps. The nozzle and device dimensions are limited by difficulties

in aligning the shadow mask used in post-printing deposition of the cathode array. However, as shown previously, printing resolutions of  $\sim 10 \mu\text{m}$  have already been demonstrated, with possible feature sizes of  $< 1 \mu\text{m}$  accessible through OVJP. Hence, improved cathode mask alignment methods should ultimately allow patterning of devices by OVJP ranging from large scale panels to micro-displays.

Though the 1<sup>st</sup> generation OVJP was extremely successful in proving that the concept of organic vapor jet printing was both viable and extremely promising, multiple design facets of the system were limiting the further progress of research. The first limitation involved the fact the mechanism to valve off sources to prevent deposition was not leak tight. As a result, there was repeated cross contamination between sources. In addition, all four sources were heated simultaneously to the same temperature. This limited the use of materials to ones that have similar sublimation temperatures. If materials with a large range of sublimation temperatures, such as BCP (sublimation temperature  $\approx 150\text{C}$ ) and NPD (sublimation temperature  $\approx 250\text{C}$ ) were concurrently put into the system problems of material degradation and uncontrollable deposition rates may occur. Also, depositing doped films in the system, though not attempted, would most likely have been difficult because instead of being able to vary both the temperature and carrier gas mass flow rate, the only changeable variable available would be the flow rate.

These limitations of the 1<sup>st</sup> generation OVJP led to design and construction of the 2<sup>nd</sup> generation OVJP meant to further the research potential of this exciting area. As seen in Figure 7 the new design includes a Blue-M convection oven to house and heat the six source cells. The inlet carrier gas enters the oven, flows through the heated source cells, and carries the inert gas/organic vapor mixture through a series of heated lines out of the

oven and into a small vacuum chamber. Inside the vacuum chamber the mixture exits through a glass nozzle that is placed in close proximity to the substrate mounted to a motorized translational stage. Each of the sources and all downstream lines are wrapped with heating tapes so that precise and individual temperature control can be maintained. Also surrounding every source are two commercial leak-tested pneumatic valves.

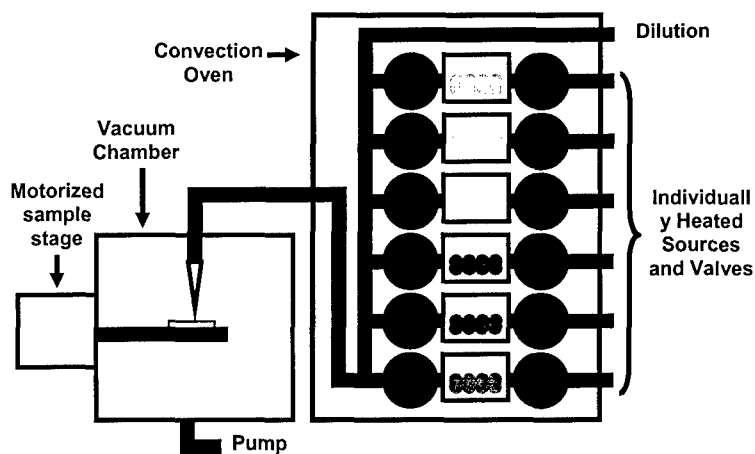


Figure 7: 2<sup>nd</sup> Generation OVJP design

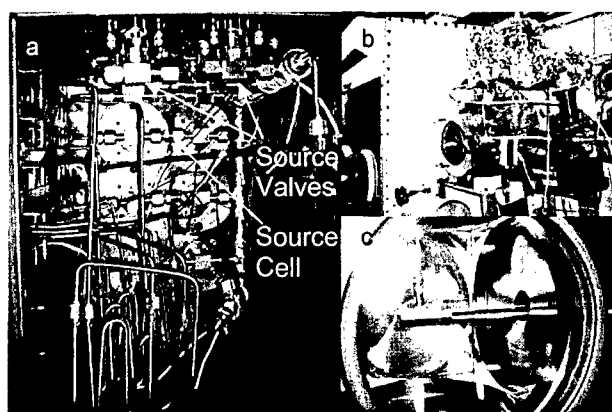


Figure 8: 2<sup>nd</sup> Generation OVJP (a) oven interior (b) vacuum chamber exterior, (c) vacuum chamber interior

Another major difference implemented in the 2<sup>nd</sup> generation OVJP is the use of a glass nozzle, created by pulling glass tubing to a taper, rather than a laser drilled metal nozzle. As seen in Figure 9, the glass nozzles have surfaces with fewer aberrations and that are much smoother, decreasing the frictional effects of the flow. In addition, the glass nozzles have the potential for extremely small apertures, even into the nanometer ranges. The 2<sup>nd</sup> generation OVJP system's Visual Basic interface controls source valves, mass flow rates, and the translational stage.

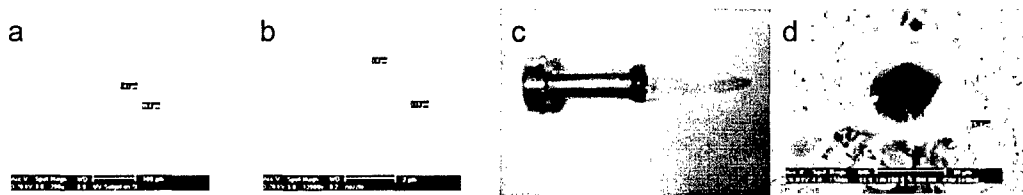


Figure 9: (a) end view 100um glass nozzle, (b) end view 3um glass nozzle, (c) side view 250um glass nozzle, (d) end view 1st generation 20 um laser driller nozzle

Currently the 2<sup>nd</sup> generation OVJP has been successful in depositing three different materials: Alq<sub>3</sub> (an electron transport material), Ir(ppy)<sub>3</sub> (a dopant for the emissive layer), and CBP (a host for the emissive layer). Alq<sub>3</sub> was deposited at 260C; Ir(ppy)<sub>3</sub> was deposited at 300C; CBP was deposited at 290C. Figure 10 shows the photoluminescence for the three materials as deposited from the OVJP. These spectra coincide with reported spectra indicating that there is no cross contamination between materials. Additionally, over up to 48 hours of leaving the system idle, there is no detectable leakage or cold spot deposition. The system has been used to deposit both flat

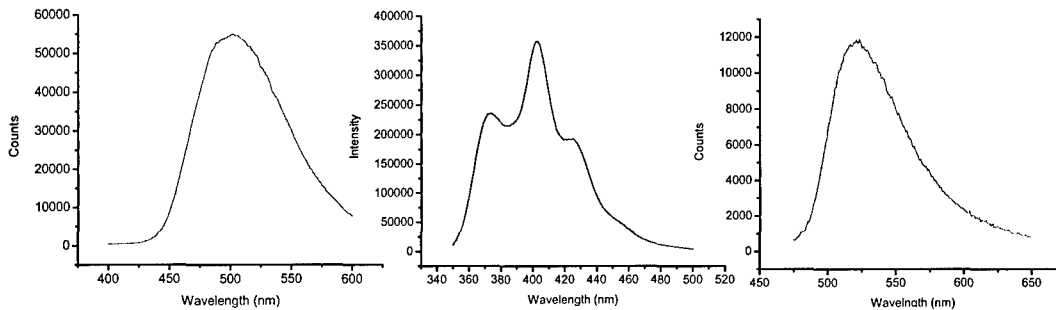


Figure 10: Photoluminescence (a) Alq3, (b) CBP, (c) Ir(ppy)3

films as well as lines using nozzles ranging from 1 mm to 250  $\mu\text{m}$  in diameter. Figure 11 and Figure 12 show the thickness and width profile of CBP lines deposited with a 1 mm diameter nozzle. As one can see, the variation in width along the length of a printed line is clearly within the error bars of the measurement. However, in Figure 8 which shows the deposition profiles of multiple lines drawn varying source mass flow rate, we can see that the FWHM of the lines varies from 1000  $\mu\text{m}$  to 600  $\mu\text{m}$ . This discrepancy in FWHM between multiple lines can be accounted for by small variations in substrate to sample distance during deposition of the lines. Figure 10 shows the Ir(ppy)3 lines deposited using a 250 $\mu\text{m}$  nozzle, at a write speed of 1.5 mm/s, and total mass flow rate of 50 sccm. This nozzle was then used to deposit a doped emissive layer of a phosphorescent OLED.

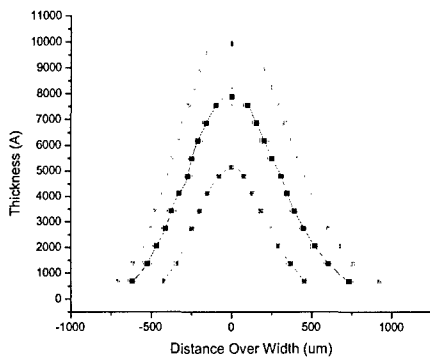


Figure 11: Thickness profiles of lines printed using source mass flow rates from 10-45 sccm

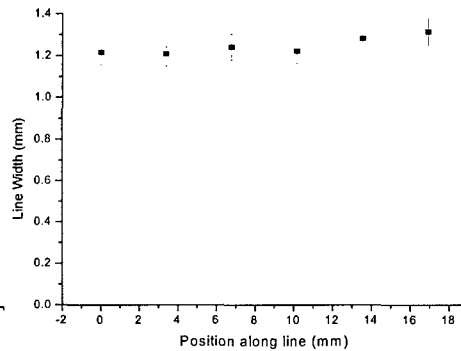


Figure 12: Width profile along length of CBP line printed with 1 mm diameter nozzle

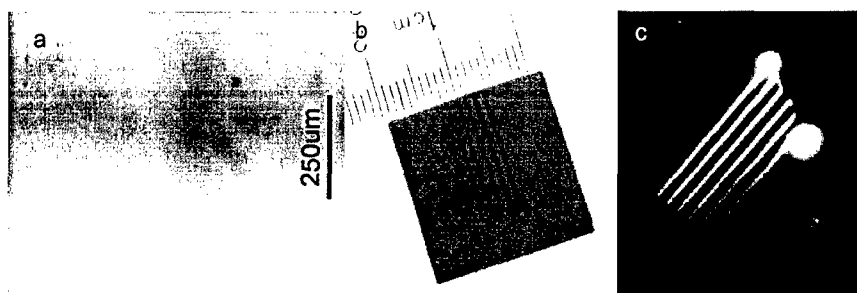


Figure 13: (a) Optical microscope picture, (b) photograph in room lighting, (c) photograph under 360nm illumination

It has been shown that in a phosphorescent OLED structure, including an Ir(ppy)<sub>3</sub> doped CBP emissive layer, by utilizing triplet relaxations the efficiency of the OLED can be dramatically improved relative to an OLED with the fluorescent emissive layer. Using the 2<sup>nd</sup> generation OVJP, we were successful in depositing a flat doped film of Ir(ppy)<sub>3</sub> in CBP. The flat film was deposited by writing back and forth, as shown in Figure 11, with a 250µm nozzle and substrate movement speed at approximately 2mm/s.

Figure 11:  
Write pattern  
for flat film.

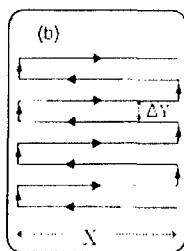


Figure 12:  
SEM of surface  
of OVJP grown  
emissive layer

Acc V Spot Magn WD P 500 nm  
10.0 kV 3.0 10000x 16.4 Glancing Angle

Scanning Electron Microscope pictures of the surface were taken as seen in Figure 12. To accurately determine dopant concentration, the CBP deposition and Ir(ppy)<sub>3</sub> deposition rates were determined separately and then combined for codeposition. It was determined that a CBP source flow rate of 12sccm, CBP source temperature of 290C, an Ir(ppy)<sub>3</sub> source flow rate of 3sccm, and an Ir(ppy)<sub>3</sub> source temperature of 300C was needed to deposit a 200Å 10% doped emissive layer. Also, a 35sccm dilution flow was added and all downstream temperatures were set at 320C to ensure the elimination of all cold spots.

As can be seen in the photoluminescence spectra in Figure 16 the doped film exhibits the absorption of the host, CBP, and the emission of the dopant, Ir(ppy)<sub>3</sub>. Also, as seen in Figure 17, in comparing the luminescence of a neat CBP film, a neat Ir(ppy)<sub>3</sub> film, and the doped film of equal thicknesses, the doped film clearly has much higher intensity emission under identical illumination as expected. Then creating the device structure as

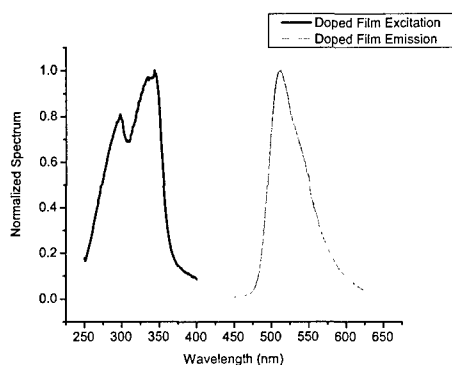


Figure 16: Photoluminescence of doped film

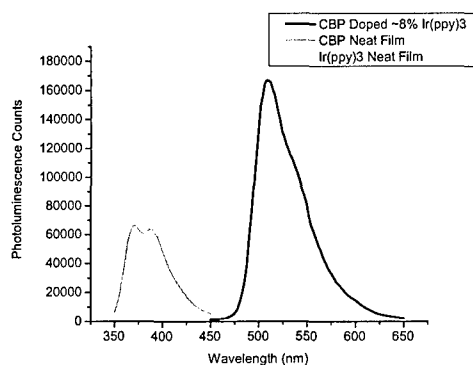


Figure 17: Photoluminescence of doped film and neat films

seen in Figure 18, the rest of the organic layers and the shadow-masked metal were deposited by vacuum thermal evaporation. The device characteristics, seen in Figures 19-22, show a peak quantum efficiency of 3.5% and power efficiency of 2.8% at 10mA/cm<sup>2</sup>. In addition the device to device and sample to sample reproducibility are adequate. In Figures 19-22, Device 1A and 1B lie on the same sample while Device 2A is from a separate OVJP deposition. At this point it is important to note that the efficiencies of the OVJP deposited phosphorescent OLED may not measure up to leading Ir(ppy)<sub>3</sub>/CBP devices due to the absence of the exciton blocking layer. It can be reasonably assumed that once this layer is introduced into the device structure, the quantum efficiency will dramatically increase to approximately 8%. Reported structures

without EBL's grown in VTE have shown quantum efficiencies around 0.2% proving the OVJP device highly competitive.

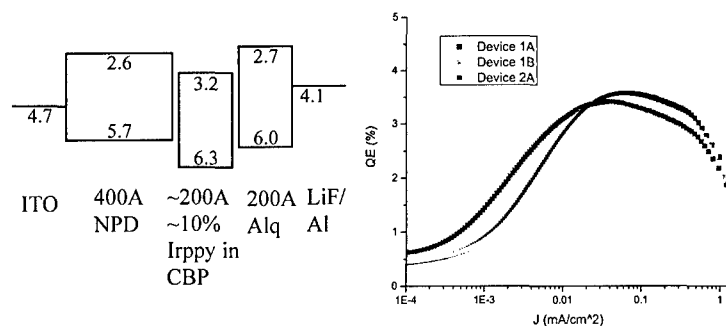


Figure 18: Device structure

Figure 19: Quantum efficiency

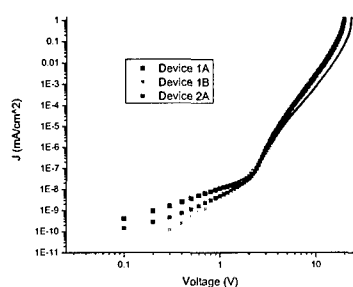


Figure 20: J-V Characteristics

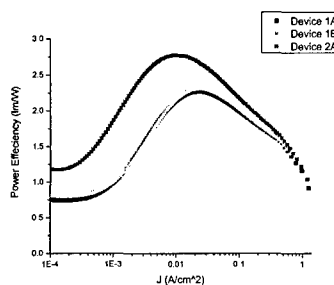


Figure 21: Power efficiency

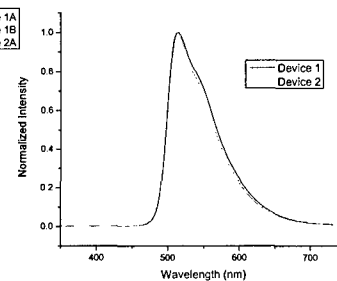


Figure 22: Electroluminescence

In addition to creating flat film devices, currently experiments are being done to achieve OVJP printed line OLED. To do this, pre-patterned ITO substrate, as seen in Figure 23 is needed to allow for individual anode contacts. In this arrangement the pre-patterned substrate would be aligned with the OVJP nozzle using multiple alignment marks. Then the OLED structure would be printed along the ITO lines followed by a shadow masking step of the metal cathode, only requiring coarse alignment. Using this method, three stripes, red, green, and blue, can be printed side by side on the same

substrate. The display applications of this feat are evident. Also, to increase deposition speed, future work plans to implement the usage of multiple nozzles side by side. As seen in Figure 24 preliminary simulations of flow patterns have been completed to model the velocity profile of the carrier gas exiting multiple nozzles. Figure 24a shows the velocity profile in the presence of only one 20 um nozzle. However, when we introduce three 20um nozzles 50 um space apart there is significant guarding of the flow. The velocity of the flow exiting the center nozzle has a much smaller component parallel to the substrate. This would result in less spreading of the deposition upon exit from the nozzle, likely leading to better resolution.

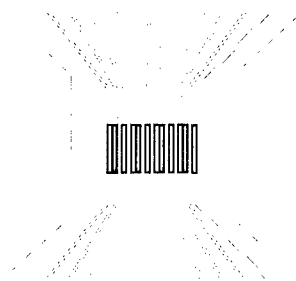


Figure 23: Pre-patterned ITO substrate for OLED stripes

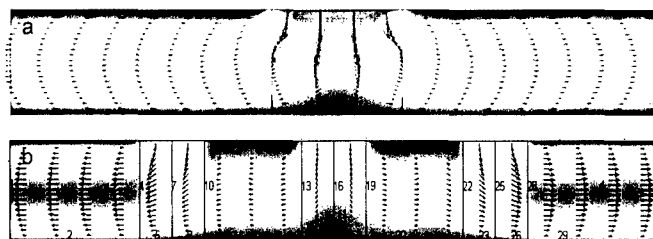


Figure 24: FEMLab simulations of carrier gas flow out of nozzle. (a) one 20um nozzle, (b) three 20um nozzles spaced 50um apart

While nozzle sizes of the 2<sup>nd</sup> generation OVJP definitely have the potential to reach the nanometer range, it is like that actually obtaining deposition profiles at the

nanometer scale will prove more difficult. Current OVJP theory predicts that the resolution of deposition is strongly dependent on the nozzle to substrate separation. To obtain depositions with nanometer resolution it is likely that it would be necessary to print at nozzle-substrate separation also in the nanometer range. Though difficult to achieve with the coarse stepper motor utilized in the 2<sup>nd</sup> generation OVJP, this separation is possible by using a surface tracking scanning microscope. Future work includes using a Near-Field Scanning Optical Microscope (NSOM) as a method of drawing these molecular wires. The NSOM uses near-field optics to exceed the resolution limit of other conventional optical microscopes. By approaching a NSOM tip very close to the sample, one is able to capture the non-propagating near field which contains higher spacial frequencies. In addition, because the NSOM tip consists of laser light coupled through the end of a tapered fiber with aperture as small as 50 nm, the resolution of the microscope is limited by the aperture size and therefore, details as small as 50 nm can be seen. In order to maintain a constant distance away from the sample, the NSOM uses tuning fork feedback methods.



Figure 25: Proposed NSOM patterning methods. (a) Near-Field Laser Ablation, (b) Near-Field Laser Deposition

By using this small aperture size and close proximity to the sample, one could potentially fabricate small organic features in two ways: 1) Near-Field Laser Ablation and 2) Near-Field Laser Deposition. These two proposed methods are illustrated in

Figure 25. The first method consists of using a high power laser coupled through the NSOM tip to burn the organic film in specific patterns. The second consists of using nanopipettes used for liquid chemical delivery and instead fill them with organic solid. Then, again, using a high power laser sublime the organic which in gas phase, will then deposit itself on the sample below. Preliminary ablation experiments have been completed on the first method. By using a frequency doubled Nd:YAG laser emitting at 532nm, 500Å pentacene films were ablated. To partially simulate the introduction of the laser into the NSOM, the laser was attenuated and then coupled into a high power fiber. At the exit of the fiber the light is focused through a series of lenses onto the VTE grown pentacene film. The substrate is housed in a nitrogen atmosphere container to prevent reaction with oxygen when ablating. As seen in Figure 26, the pentacene films were successfully ablated using powers ranging from 10W-1kW for exposure times ranging from 1-10 seconds. The SEM pictures show a slight collection of material on the edge of the ablated region. This may be due to redeposition of the pentacene molecules after they are ablated. Performing these experiments in vacuum may decrease this effect.



Figure 26: Ablation Experiments (a) optical microscope picture of ablated dot, (b) SEM picture of ablated dot, (c) SEM zoom in of center of ablated dot.

Organic semiconductor patterning is becoming more and more important the advancement of organic electronics. By being able to directly pattern onto substrates, we are able to bypass lengthy and costly alignment steps for the fabrication of many devices

such as full color displays and transistors. While the 1<sup>st</sup> generation OVJP showed great promise for the technology of vapor printing, 2<sup>nd</sup> generation system has been proven to be able to achieve more complicate device structures, opening new avenues for exciting research. Future projects affiliated with OVJP include the creation stripe OLEDs as well as the introduction of multiple nozzles. However, in order to achieve resolution down to the nanometer scale, the integration of the OVJP technology with new ultra high resolution microscopes, such as Near-Field Scanning Optical Microscopy, may be necessary. As we delve further into the nanometer resolution deposition, many doors are open to new device structures and arrangements. Without a doubt, OVJP and other organic patterning methods are crucial to the success of organic semiconductors and there integration into the mainstream market.